Desalination and Water Treatment
www.deswater.com

doi: 10.5004/dwt.2020.26433

207 (2020) 300–308
December

Fabrication of geopolymer microspheres and their Pb(II) adsorption performance by fixed-bed column method

Sijie Yang, Yan He*, Guohui Xue, Haoyang Yu, Xuemin Cui*

Guangxi Key Laboratory of Petrochemical Resource Processing and Process Intensification Technology, School of Chemistry and Chemical Engineering, Guangxi University, Guangxi, Nanning 530004, China, emails: 568158886@qq.com (Y. He), cui-xm@tsinghua.edu.cn (X. Cui), 308557558@qq.com (S. Yang), 2474117981@qq.com (G. Xue), 942346331@qq.com (H. Yu)

Received 25 February 2020; Accepted 6 August 2020

ABSTRACT

This paper dedicated a simple preparation processing of metakaolin-based geopolymer microspheres (MGMs) by the means of suspension dispersion solidification method (SDS), and explored the effects of dimethyl silicone oil temperature and stirring speed on the particle size distribution of MGMs. The prepared MGMs were characterized by X-ray diffraction, scanning electron microscopy, and Brunauer–Emmett–Teller methods. The results showed that MGMs were provided with perfect spherical shape and with a controllable diameter range within 25–450 μm. The MGMs demonstrated excellent adsorption performance for Pb(II) from water. Herein, the following study discussed the engineering applications of fixed bed adsorption technique, including the effect of different flow rate, the particle size of MGMs, bed height, and initial Pb(II) concentration on the breakthrough curves, by using MGMs for Pb(II) removal from aqueous solution.

Keywords: Geopolymer; Metakaolin-based microspheres; Suspension dispersion solidification; Fixed bed adsorption

1. Introduction

Geopolymer [1] is a type of low-cost green inorganic non-metallic material with an amorphous or quasi-crystalline three-dimensional network gel structure. Geopolymers have excellent properties including high compressive strength, great acid, and heat resistance [2]. Due to these excellent properties, geopolymers are widely applied in building materials [3], pH buffering [4], absorbent, or immobilization of toxic waste [5,6]. At present, many researchers make use of fly ash, slag, metakaolin, or other industrial wastes to synthesize geopolymers, which not only realized the recycling of wastes but also develop many types of engineering materials [7–9].

With the rapid expansion of industry, many environmental pollutions, particularly heavy metal contamination that resulted in a serious threat to life and nature. The treatment of heavy metal pollution has become one of the most urgent problems around the world. Currently, methods for treating heavy metal ion contamination include chemical precipitation, electrolysis, membrane separation, and adsorption [10], etc. Adsorption is the most widely process owing to its high efficiency, cost-effectiveness, and simple procedure [11].

At present, the emerging adsorbents are various, but most of them are powdery [12–16]. In the practical application process, it is difficult to separate the powder material from the adsorption liquid, and the flow resistance is high, which is not conducive to continuous operations [17]. Fortunately, the suitable spherical adsorbents with a low flow resistance are easy to disassemble and separate, which can overcome the drawbacks of powder adsorbents and facilitate continuous operations. Therefore, the simple, low-cost, and environmentally friendly preparation process of spherical adsorbents is eagerly called out.

* Corresponding authors.

In principle, the methods of spherical particle materials synthesis include ultrasonic spray pyrolysis [18], microfluidic [19], and suspension solidification [20], etc. The spherical particle materials obtained by the spray pyrolysis method have these properties of weeny particle size, uniform mesoporous distribution, and environmental-friendly synthesis process [18,21]. The microspheres, which are obtained by microfluidic approach, have approximate uniform particle size. Different particle sizes of microspheres will achieve by changing the thermodynamic properties of fluids, while this approach is time-consuming and microfluidic chips are extremely expensive, and chips will be scrapped if they become occlusion [22]. Suspension solidification method is suitable but inefficient for preparation of MGMs with great spherical and a narrow particle size distribution ranging from 200 to 300 μm [23]. The efficiency of preparing microspheres has been improved remarkably by using SDS method in this study, which is an improvement of suspension solidification method.

At present, adsorbents for heavy metal removal can be classified into natural adsorbents, synthetic adsorbents, and biological adsorbents according to their sources. According to different application environments, various types of geopolymer adsorbents have appeared, such as powders, porous spheres, and so on. Metakaolin-based geopolymers have been studied for the adsorption of NH_4^+ from model solutions and landfill leachate and heavy metals from aqueous solution [24,25]. Cheng et al. [26] focused on adsorbing different heavy metal including Pb(II), Cu^{2+}, Cr^{3+}, and Cd^{2+} via metakaolin-based geopolymer powders under various experimental conditions and reported that metakaolin-based geopolymers have the property of adsorbing heavy metal ions. In addition, Kara et al. studied Mn^{2+}, Co^{2+}, Zn^{2+}, and Ni^{2+} removal from aqueous solutions by using metakaolin-based geopolymer powder and the result showed that the Langmuir adsorption isotherm was verified to be 72.34, 69.23, 42.61, and 74.10 mg/g for Mn^{2+}, Co^{2+}, Ni^{2+}, and Zn^{2+}, respectively [14,15]. Tang Qing et al. [20] synthesized metakaolin-based spheres with a particle size of 200–300 μm to adsorb Cu^{2+}, Pb(II), and Ca^{2+}, and the equilibrium adsorption capacities were 34.5, 45.1, and 24.0 mg/g, respectively. In addition, slag-based porous geopolymer microspheres have high selective adsorption ability for Pb(II) and outstanding adsorption capacity as high as 629.21 mg/g [27].

Herein, inspiring the suspension solidification method, we developed a suspension dispersion solidification (SDS) method which was applied in this study to fabricate MGMs with perfect sphericity and poly-dispersed particles. Most importantly, silicone oil and metakaolin utilizing in this study are not only inexpensive and the silicone oil can be reused.

2. Materials and characterizations

2.1. Materials

The metakaolin used in this work was provided by Chaopai Company, Inner Mongolia of China. The chemical components of the metakaolin were listed in Table 1, which composition was tested by X-ray fluorescence (XRF). Water glass with an industrial-grade was provided by Guangxi Chunxu Chemical Company, China. The module rate (SiO_2/Na_2O molar ratio) and solid content of water glass were 3.31 and 38.7 wt.%, respectively. The industrial-grade dimethyl silicone oil with a kinematic viscosity of 2,000 mm^2/s. Analytical grade sodium hydroxide with a content of 96.0 wt.%, $Pb(NO_3)_2$ were used.

Table 1
Content of metakaolin (wt.%)

Element	Content, %
Ca	0.150
Si	23.810
Fe	0.420
K	0.220
Mg	0.066
S	0.730
Al	23.820

2.2. Characterizations

The specific surface area of MGMs was tested by Micromeritic Gemini 2390 surface area and porosity analyzer (America). Hitachi S-3400N scanning electron microscopy (SEM) (Japan) was used to observe the roundness and sphericity of MGMs, and the elemental content was analyzed using energy dispersive analysis (EDS, EDAX PV8200) (Japan). The crystalline phases of MGMs were identified via Rigaku MiniFlex 600 X-ray diffractometer (XRD) (Japan) with a CuKα source operating at 40 kV and 15 mA. The scanning range (2θ) was from10° to 70°, at a step size of 0.02° and a rate of 10°/min. The concentration of a lead ion in solution was determined by inductively coupled plasma emission spectrometer (ICP, Thermo Fisher ICAP 6300), carrier gas flux of 0.5 L/min, with radio-frequency power of 1,150 W, the peristaltic pump of 50 rpm and auxiliary air flux of 0.5 L/min. Shaker (QYC-200) was supplied by the Shanghai Fuma Experimental Facilities Company. The pH was measured by pH Meter (PHS-3C, Shanghai).

2.3. Preparation

Geopolymer pastes with a mass ratio of metakaolin: water glass (1.3 Module) = 0.94, H_2O/Na_2O molar ratio = 18 were obtained through mixed metakaolin and water glass (1.3 Module) at a speed of 2,000 rpm for 6 min, which was then immediately poured into a syringe. One-thousand milliliters of silica oil (continuous phase) was heated to 50°C, 60°C, 70°C, and 80°C, respectively, and stirred by a dispersion machine. The slurry was injected into silica oil and broken into small droplets under the viscous shear force of silica oil or agitator blade. And the slurry droplets gradually formed their spherical shape resulting from surface tension and solidified in the process of falling in high-temperature silicone oil. Agitation speeds were controlled at 500, 600, 700, and 800 rpm, respectively, so as to obtain droplets with different diameters. Fully solidified MGMs were collected and the silica oil on the surface was washed with distilled water and then dried at 60°C. Finally, the spheres were sintered for 6 h at 450°C to clean

off the remaining silica oil on the surface and in the pores MGMs. The preparation process is shown in Fig. 1.

2.4. Adsorption experiments

2.4.1. Batch adsorption experiments

0.1 g MGMs adsorbents were separately added into three Erlenmeyer flasks with 100 mL ion concentrations of $C_{Pb(II)}$ = 200 mg/L at pH = 5. The Erlenmeyer flasks were placed into a shaker with a shaking speed of 250 rpm at 25°C for 48 h. Then, the samples were taken out and tested via ICP for Pb(II) concentration. The adsorption capacities (Q_t) of geopolymers microspheres were calculated with the following equation:

$$Q_t = \frac{V\left(C_0 - C_e\right)}{m} \tag{1}$$

where V (L) is the volume of the lead ions solution; C_0 and C_e (mg/L) are the initial and final concentrations of metallic ions respectively; and m (g) is the mass of MGMs adsorbents.

2.4.2. Fixed bed adsorption experiments

The fixed bed adsorption experiments were conducted in a quartz column (1.0 cm internal diameter × 8.0 cm height), as shown in Fig. 2. A certain amount of MGMs adsorbents were packed in the quartz column, the bed layer was covered with nylon mesh at the top and bottom to prevent the adsorbent from being washed away. The lead ions solution (pH = 5) was pumped into the quartz column from the bottom at different inflow rate (1, 2, and 3 mL/min), initial lead ions concentration (200, 100, and 20 mg/L), fixed-bed length (1, 2, and 3 cm) and particle size of MGMs (100–150, 150–200, and 200–400 μm) using a peristaltic pump at room temperature. The effluent samples were collected from the top of the column at different time intervals and the concentration of the samples were measured via ICP.

2.4.3. Fixed bed column data analysis

The fixed bed adsorption experiments can be evaluated by breakthrough curves, which is to plot the time (t) with the experimental data concentration (C_t/C_0) at the ratio of effluent to inflow. From the breakthrough curves of the fixed bed, the breakthrough time (t_b) and the saturation time (t_s) were measured when C_t/C_0 = 0.1 and C_t/C_0 = 0.9, respectively [17].

The amount of metal adsorbed in the breakthrough process can be employed by Eq. (2):

$$M_{ad} = M_{in} - M_{out} \tag{2}$$

where M_{in} (mg) uptake amount of metal entering the column reactor in the whole fixed-bed adsorption process and is expressed as:

$$M_{in} = C_0 Q_t \tag{3}$$

where M_{out} (mg) denoted amount of unadsorbed metal eluting from the fixed bed and is expressed as:

$$M_{out} = C_0 Q \int_0^t \left(C_t - C_0\right) dt \tag{4}$$

where C_0 (mg/L) represents the concentration of lead ions in the influent, Q (L/min) is the flow rate, C_t (mg/L) is the concentration of lead ions in the effluent after adsorption for t, min.

The adsorption capacity of the sorbent can be calculated as follows:

$$Q_{tf} = \frac{M_{ad}}{m} \tag{5}$$

where m (g) is the mass of sorbent.

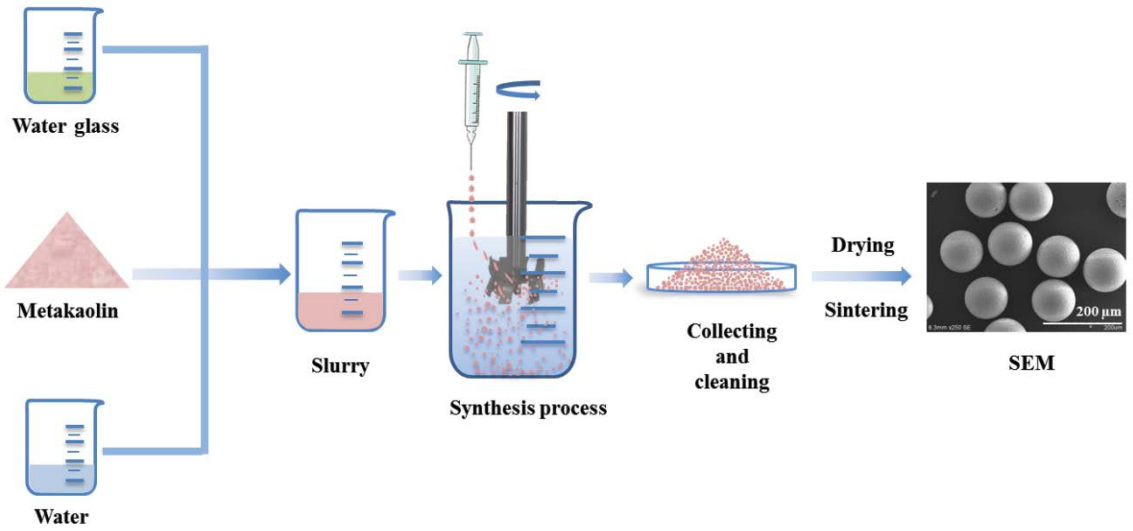

Fig. 1. Preparation scheme of porous inorganic spheres with the SDS method.

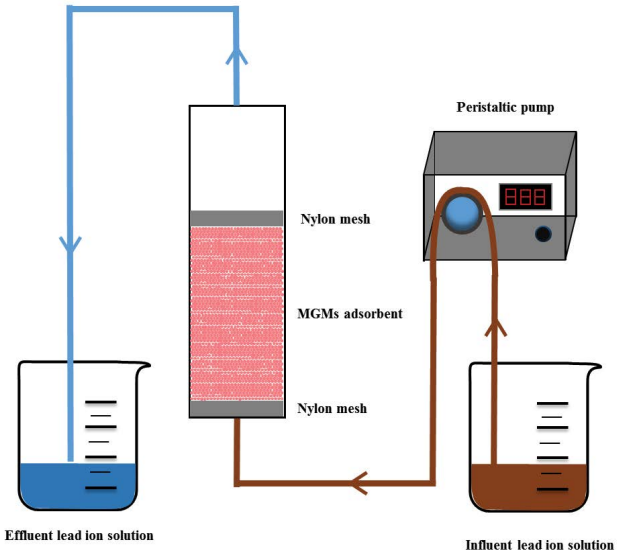

Fig. 2. Schematic representation of the apparatus arrangement in fixed-bed column experiments.

The adsorption efficiency which determines how clean the treated effluent can be calculated as follows:

$$R = \frac{M_{ad}}{M_{in}} \times 100\% \quad (6)$$

3. Results and discussion

3.1. MGMs fabrication mechanism

The dispersion of the droplets comes from two aspects were agitator blade crushing and viscous shear force crushing in the dispersion area. The crushing from the agitator blade is shown in Fig. 3a. When continuous slurry was injected into the silicone oil, and then the slurry was drawn into the vortex with the silicone oil moving and be crushed due to the kinetic energy of the blade. The slurry droplets collide with the blades rotating at high speed and were broken into a plurality of sub-droplets with different sizes. The sub-droplets are thrown out of the dispersion center region with the continuous phase moves, and then move around into the sedimentation area.

The crushing from the viscous shear force is shown in Fig. 3b. As the velocity gradient exists in the radial direction of the blades, the velocity on the different streamlines was different. With the viscous shear force generated by the flow of the continuous phase, the large volume droplets of slurry across the flow lines of different flow were elongated and broken into small droplets. Subsequently, the small droplets gradually moved away from the central area of the agitator blade with the movement of silicone oil and enter the sedimentation area.

It can be seen that in the SDS method, the stirring speed have a great influence on the particle size, distribution, and sphericity of the MGMs. This work focused study on the stirring speed and the temperature of silicone oil in order to get the dispersion rule, and obtain the processing parameters that can efficiently fabricate MGMs.

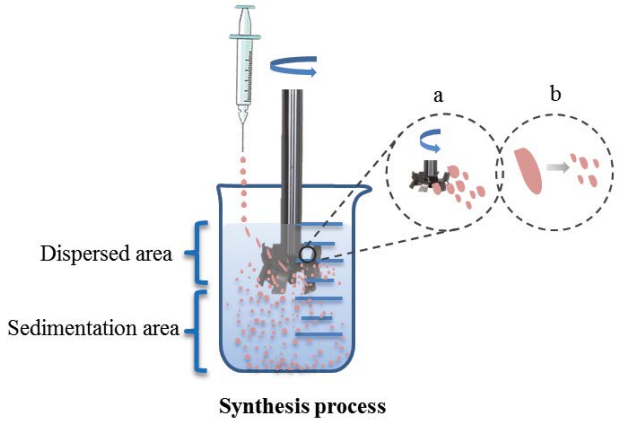

Fig. 3. Regional distribution of the reactor and Crushing schematic of droplets, (a) crushing from the agitator blade, (b) crushing from the viscous shear force.

3.2. Influence of stirring speed on particle size distribution

From the experimental results of Fig. 4, with the increase of stirring speed from 500 to 800 rpm, the proportion of small particle size of MGMs increases gradually. When the stirring speed is equal to 700 and 800 rpm, the proportion of MGMs (25–75 μm) reaches 81.48% and 84.50%, respectively, while the large size (200–450 μm) MGMs proportion only occupy 0.64% and 0.35%, respectively. When the stirring speed was 500 rpm, the proportion of large-diameter MGMs (200–450 μm) was much higher than that of other stirring speeds.

The homogeneous slurry was dispersed into droplets, and the MGMs size was highly relative to stirring speed. Smaller size of MGMs was obtained using a high stirring speed; oppositely, bigger MGMs would be generated. The impeller can provide bigger viscous shear force lead to greater kinetic energy for slurry and break it into smaller and more droplets with the increase of stirring speed. In addition, the higher the stirring speed, the greater the radial velocity difference near the blade, even small droplets, would be broken into smaller size droplets due to the region across different velocity. Therefore, with the increasing of stirring speed, the MGMs proportion of fine particles increases. The maximal mass of microspheres with the target size (75–125 μm) was obtained at 500 rpm which was the reason for choosing 500 rpm as the optimum stirring speed for the preparation of microspheres.

3.3. Influence of temperature on particle size distribution

Temperature of silicone oil is one of the key factors, which can affect the particle size of MGMs. It can be seen from Fig. 5, with the increase of silicone oil temperature, the content of the MGMs with large particle size increased while the small size decreased. At 50°C, the distribution of particle size of MGMs was uniform. However, the MGMs (200–450 μm) of the large-diameter were as high as

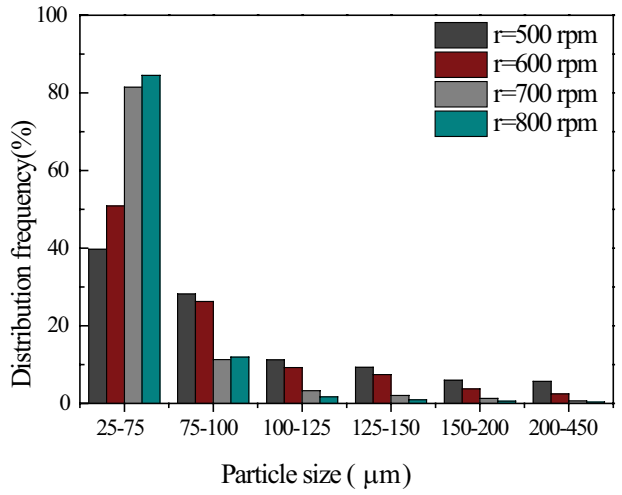

Fig. 4. Influence of stirring speed on particle size distribution.

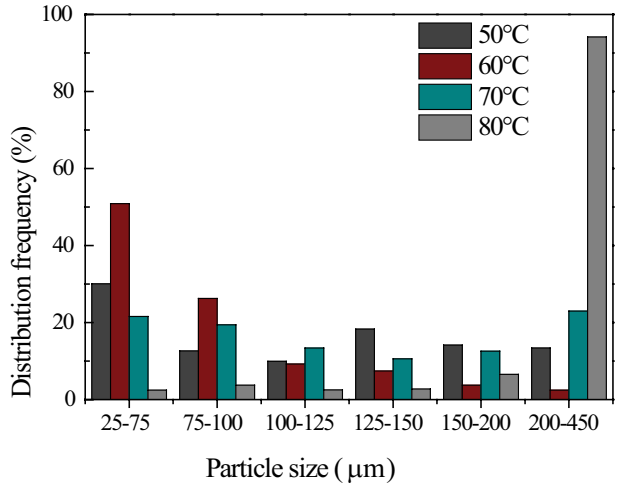

Fig. 5. Influence of temperature on particle size distribution with 500 rpm.

94.17% at 80°C, while its small diameter (25–75 μm) only contained 2.45%.

The solidification time of MGMs is directly affected by the temperature of silicone oil. Because the geopolymerization is rapid then the solidified time is short at a high temperature. On the contrary, the reaction rate is slow and the curing time is long at low temperature [28]. Droplets may solidify before they are spheridized in the dispersed area, and the droplets will coalesce with other droplets and solidify before they can be separated, which lead to a sharp increase in the proportion of large-sized MGMs at 80°C. The results show that high temperature is not conducive to the preparation of MGMs.

The process of being thrown out of the dispersion area is momentary after the slurry was dispersed into small droplets, which have not yet solidified at 50°C. At this point, the uncured droplets that have fallen to the bottom of the reaction vessel were stacked on each other, extruded, and solidified in this state. While the spherical droplets can be solidified before they fall to the bottom of the reactor when the temperature (60°C) of the silicone oil was suitable. The MGMs would not be deformed and adhered, and still maintain good sphericity even if MGMs were stacked and pressed on the bottom of the reactor. This was the reason why the proportion of large-sized (150–200 μm) MGMs at 50°C was larger than that of 60°C. In summary, 60°C adopting in this study was the suitable temperature for the preparation of MGMs.

3.4. Specific surface area and pore structure analysis

Specific surface area is a vital performance of adsorbents. Generally, the larger the surface area of MGMs, the more active adsorption sites for adsorbates [27]. The reaction temperature directly affects the specific surface area of the MGMs (Fig. 6). With the increase of silicone oil temperature, the specific surface area of MGMs increased first and then decreased. It can be explained that appropriately increasing the reaction temperature (50°C–60°C) can enhance the reaction speed and improve the physical properties of MGMs. Whereas, too high temperature (70°C–80°C) causes too fast a curing rate and produces a negative influence that the geopolymer gel will cover the metakaolin particles that are not dissolved and prevent further geopolymerization [28]. It can be concluded that the MGMs obtained at the reaction temperature of 60°C has the largest specific surface area, which is another reason for chose 60°C as the reaction temperature in this work.

3.5. XRD and SEM analysis

As can be seen from Fig. 7, the XRD pattern of metakaolin with a wide hump in 15°–30° demonstrated the metakaolin with amorphous structure. The XRD pattern of unsintered MGM exhibits a wide dispersion peak near 15°–35°, displaying the amorphous structure without crystal. Comparing the XRD pattern of metakaolin and MGMs, it can be concluded that metakaolin has been converted into geopolymer. Besides the XRD patterns of sintered MGMs and unsintered MGMs were almost identical indicating that the amorphous structure of MGMs did not change. Therefore, the redundant silica oil in MGMs was completed removed via sintering at 450°C for 6 h.

The SEM micrographs of MGMs with a diameter of approximately 100 μm are shown in Fig. 8. The MGMs have an excellent sphericity that displays in Figs. 8a and b. There are many pore structures shown in Figs. 8b and c, which may reduce the resistance of heavy metal ions to diffuse into MGMs and promote the adsorption process of heavy metal ions by MGMs.

3.6. Adsorption studies

3.6.1. Batch adsorption studies

MGMs (prepared by 500 rpm at 60°C) were washed to be neutral (pH = 7.0) via distilled water before adsorption experiment. The pH of Pb(II) ions solution was adjusted to 5 by 0.1 mol/L NaOH or HNO_3. The adsorption capacity for Pb(II) is 174.1 mg/g. It demonstrated that the

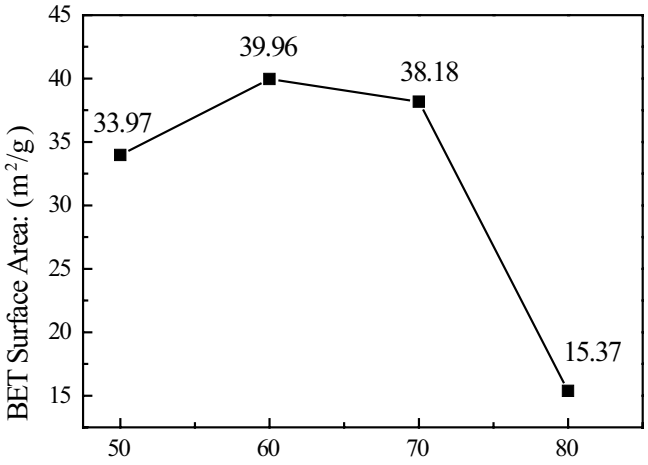

Fig. 6. Influence of temperature on the surface area of MGMs with 500 rpm.

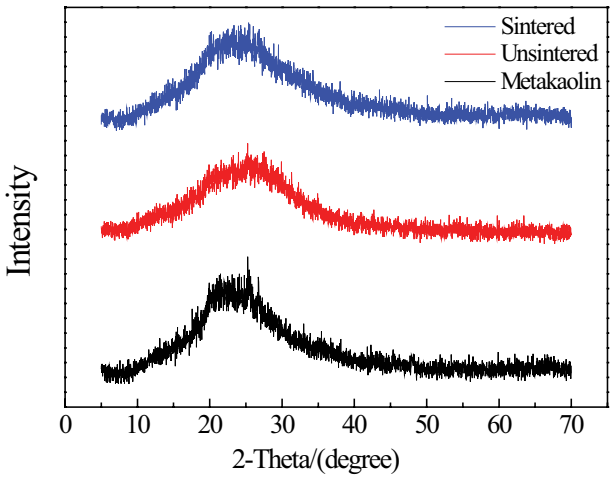

Fig. 7. XRD patterns of metakaolin, unsintered, and sintered MGMs.

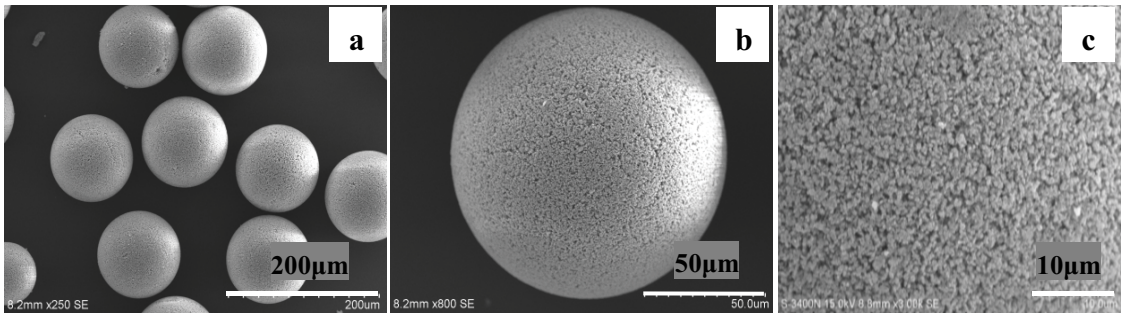

Fig. 8. (a) Image of MGMs, (b) surface morphology of MGM, and (c) enlarged image of (b).

adsorb Pb(II) ability of porous MGMs is excellent and it is feasible to utilize MGMs to adsorb lead ions. Herein, the results of the batch adsorption experiments provide a theoretical basis for the fixed bed adsorption experiments. Since the latter experiments take Pb(II) for fixed-bed adsorption.

The adsorbed Pb(II) MGMs were broken and then analyzed by EDS so as to investigate the diffusion of Pb(II) in MGMs. It is obvious that Pb(II) ions have diffused into the interior of MGMs shown in Fig. 9. It can be interpreted as MGM has a large number of pore structures, which is also consistent with the previous SEM analysis.

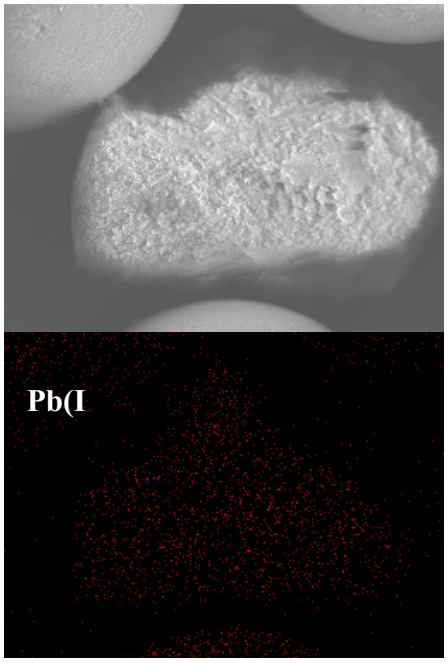

Fig. 9. Distribution of lead elements on the internal cross-section.

3.6.2. Fixed bed adsorption studies

In this section, the effects of different flow rate, particle size of MGMs, bed height, and initial Pb(II) concentration on the fixed adsorption of Pb(II) by MGMs were investigated. The experimental conditions and results are shown in Table 2.

3.6.2.1. Effect of flow rate on breakthrough curves

The flow rate is one of the key factors affecting the breakthrough curve, and the influence of different flow

Table 2
Parameters for Pb(II) removal by MGMs in the fixed bed under different operating conditions

Flow rate (Q) (mL/min)	Bed height (h) (cm)	Initial concentration (C_0) (mg/L)	Particle size of MGMs (d) (μm)	Adsorption capacity (Q_{tf}) (mg/g)	Percentage adsorption (R) (%)	Breakthrough time (t_b) min	Saturation time (t_s) min
1	1	200	150–200	246.4	45.3	136	720
2	1	200	150–200	131.8	50.2	72	480
3	1	200	150–200	75.2	41.5	36	240
2	2	200	150–200	105.3	57.4	70	420
2	3	200	150–200	123.5	75.8	336	720
2	1	100	150–200	123.4	46.5	142	630
2	1	20	150–200	130.3	51.8	852	3,360
2	1	200	200–400	81.7	33.4	50	360

rates on the fixed bed adsorption of Pb(II) by MGMs is shown in Fig. 10a. At the flow rate of 1 and 2 mL/min, the breakthrough time are 136 and 72 min, respectively, and the saturation time were 720 and 480 min, respectively. As the increase of flow rate, the slope of the breakthrough curve increases, and the saturation time is shortened. When the flow rate rises to 3 mL/min, the breakthrough time is shortened to 35 min and the saturation time increased to 360 min. This is because the higher the flow rate is, the faster the Pb(II) solution passes through the fixed bed, the shorter the contact time of the Pb(II) solution with the MGM adsorbent, and the active adsorption sites are not fully utilized [29,30]. As a result, the slope of the breakthrough curve increases, the saturation time is shortened, and the adsorption amount is reduced. On the contrary, the lower the flow rate is, the smaller the driving force and the slower the Pb(II) solution passes through the fixed bed. The longer the contact time between the Pb(II) solution and the MGM adsorbent is, the more active adsorption sites are fully utilized. Therefore, under the flow rate of 1 mL/min, the adsorption capacity of MGM to Pb(II) is the largest. However, very low flow rate often leads to adverse reflux, which reduces the removal efficiency of Pb(II) per unit time [17]. Therefore, 2 mL/min flow rate is adopted in subsequent experiments.

3.6.2.2. Effect of particle size of MGMs on breakthrough curves

The effect of particle diameter on the bed bulk density is the most obvious [31]. In this experiment, two kinds of MGMs adsorbents with different particle sizes are used for filling the fixed bed and the experimental results are shown in Fig. 10b. It can be seen that the fixed bed filled with MGMs of 200–400 μm is reduced to a fixed bed filled with MGMs of 150–200 μm, the breakthrough time is increased from 50 to 72 min, and the saturation time is increased from 360 to 480 min. It is indicated that the use of different particle sizes MGMs to fill the fixed bed has different diffusion resistance. MGMs with different particle size ranges were obtained in this experiment, and then the diffusion resistance can be adjusted by filling MGMs of different particle sizes in practical applications. The reason of this result is that the porosity of the packed bed of large particle size MGMs is larger than that of the small particle size, and the diffusion resistance of the lead solution in the fixed bed filled with large particle size is smaller than that of the small particle size, resulting the driving force is larger than that of the small particle size and cannot be sufficiently contacted with the active adsorption site of the MGMs [31]. Therefore, the adsorption capacity and removal rate of Pb(II) in the fixed bed filled with large particle sizes are smaller than those in the small particle size. The MGMs with d = 150–200 μm were used for filling the fixed bed in the subsequent experiments.

3.6.2.3. Effect of bed height on breakthrough curves

Bed height is a vital design parameter of the tower reactor, which determines the amount of adsorbent and affects the quality of wastewater treatment, because the number of metal-binding sites is directly related to the amount of adsorbent [17,29]. The effect of bed height on breakthrough curves as shown in Fig. 10c, the slope of breakthrough curves decreases with the increase of MGMs dosage. With the increase of bed height from 1.0 cm (MGMs dosage is 0.5452 g) to 3.0 cm (MGMs dosage is 1.6356 g), breakthrough time increases from about 70 to 336 min, saturation time extends from 420 to 720 min, adsorption capacity decreases from 131.8 to 123.5 mg/g, but the removal rate increases from 50.2% to 75.8%, signifying that the bed lengths strongly affected the adsorbed process. The contact time between MGMs and Pb(II) increases with the increase of bed height, thus prolonging the breakthrough time and saturation time. In addition, the length of the mass transfer zone increases with the height of the packed bed, which leads to an increase in the number of binding sites (from 0.5452 to 1.6356 g), and improves the total adsorption capacity and the removal efficiency of Pb(II). Other studies have reported similar trends [29,30,32]. Since excessive MGMs results in higher bed pressure, subsequent experiments were conducted at a bed height of 1.0 cm.

3.6.2.4. Effect of initial Pb(II) concentration on breakthrough curves

The effect of initial Pb(II) concentration on breakthrough curves is shown in Fig. 10d and Table 3, which

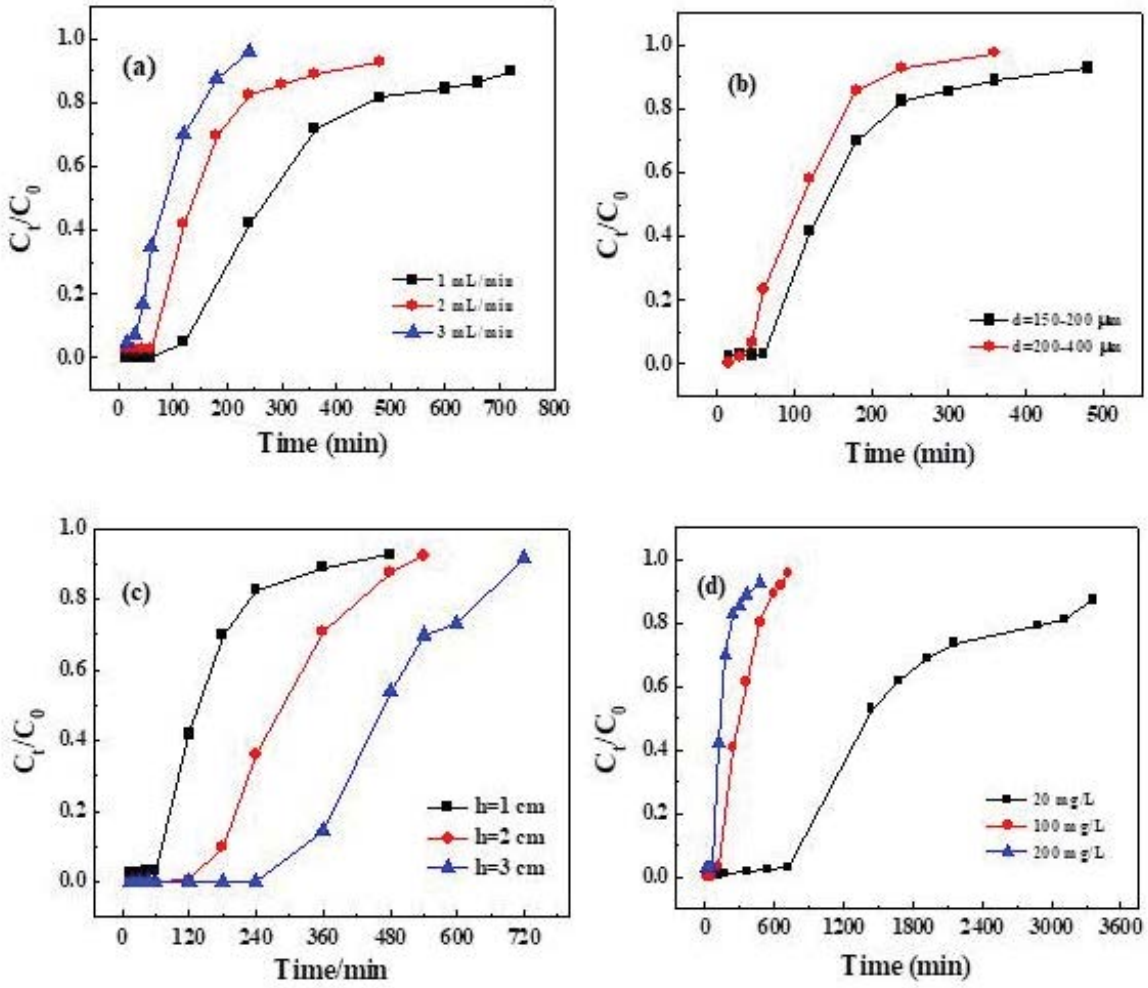

Fig. 10. (a) Effect of inflow rate on breakthrough curves of lead ions adsorption onto MGMs (pH = 5, h = 1 cm, d = 150–200 μm, C_0 = 200 mg/L), (b) effect of particle size of MGMs on the breakthrough curve of lead ions adsorption onto MGMs (pH = 5, h = 1 cm, Q = 2 mL/min, and C_0 = 200 mg/L), (c) effect of fixed-bed length on the breakthrough curve of lead ions adsorption onto MGMs (pH = 5, Q = 2 mL/min, d = 150–200 μm, and C_0 = 200 mg/L), (d) effect of initial lead ions concentration on the breakthrough curve of lead ions adsorption onto MGMs (pH = 5, Q = 2 mL/min, d = 150–200 μm, and h = 1 cm).

indicates the change of initial concentration of Pb(II) from 20 to 200 mg/L greatly affects the breakthrough curve. With the increase of the initial concentration of lead ion, the breakthrough and adsorption saturation time are greatly shortened. From 20 to 200 mg/L, the breakthrough curve becomes sharper, and the breakthrough time decreases from about 852 to 70 min and saturation time also decreases from 3,360 to 480 min demonstrating that MGMs shows good durability at low Pb(II) concentration. In a lower concentration of Pb(II), the extension of breakthrough point, due to the lower mass transfer in the adsorption process leading to more treatment of Pb(II) solution. On the contrary, the higher concentration gradient provides a larger mass transfer driving force, manifesting that the adsorption rate increases with the increasing of initial Pb(II) concentration and leading to a faster saturation of the adsorption process, which can be explained by more feed of Pb(II) solution per unit surface area of MGMs [17].

4. Conclusions

In this study, the controlled diameter and sphericity of geopolymers microspheres were prepared using SDS method. The standard sieve results showed that metakaolin-based geopolymer microspheres (MGMs) with controllable diameter range within 25–450 μm and the fixed bed adsorption indicated that the use of different particle sizes MGMs to fill the fixed bed has different diffusion resistance. Experimental results showed that stirring speed and temperature are the main factors affecting the particle size distribution of MGMs, and the temperature of dimethyl silicone oil also impacted on Brunauer–Emmett–Teller surface area of the microsphere. It was best to prepare MGMs when the temperature of silicone oil was 60°C and the stirring speed equal to 500 rpm. The analysis of SEM exhibited that there are perfect sphericity of the MGMs. Besides, batch adsorption test and ICP analysis also suggested that

the MGMs possess great removal efficiency for Pb(II). The flow rate, particle size of MGMs, bed height, and initial Pb(II) concentration impacted the breakthrough curve of Pb(II) adsorption onto MGMs in the fixed bed column. The increase in fixed-bed column length, initial concentration, and the decrease in particle size of MGMs and flow rate improved the adsorption performance and may be effectively applied for the removal of metal ions from wastewater.

Acknowledgments

This work was supported by the Chinese Natural Science Fund (grant no.: 51772055), the Guangxi Natural Science Fund (grant no.: 2016GXNSFGA380003).

References

[1] J. Davidovits, Geopolymers and geopolymeric materials, J. Therm. Anal., 35 (1989) 429–441.
[2] P.G. He, M.R. Wang, S. Fu, D.C. Jia, S. Yan, J.K. Yuan, J.H. Xu, P.F. Wang, Y. Zhou, Effects of Si/Al ratio on the structure and properties of metakaolin based geopolymer, Ceram. Int., 42 (2016) 14416–14422.
[3] G.S. Wang, Y.W. Ma, Drying shrinkage of alkali-activated fly ash/slag blended system, J. Sustainable Cem.-Based Mater., 7 (2018) 203–213.
[4] R.M. Novais, M.P. Seabra, J.A. Labrincha, Porous geopolymer spheres as novel pH buffering materials, J. Cleaner Prod., 143 (2017) 1114–1122.
[5] Y. Zhang, P.G. He, J.K. Yuan, C. Yang, D.C. Jia, Y. Zhou, Effects of graphite on the mechanical and microwave absorption properties of geopolymer based composites, Ceram. Int., 43 (2017) 2325–2332.
[6] B.L. El-Eswed, O.M. Aldagag, F.I. Khalili, Efficiency and mechanism of stabilization/solidification of Pb(II), Cd(II), Cu(II), Th(IV) and U(VI) in metakaolin based geopolymers, Appl. Clay Sci., 140 (2017) 148–156.
[7] S. Onutai, T. Kobayashi, P. Thavorniti, S. Jiemsirilers, Porous fly ash-based geopolymer composite fiber as an adsorbent for removal of heavy metal ions from wastewater, Mater. Lett., 236 (2019) 30–33.
[8] Q. Tang, G.-H. Xue, S.-J. Yang, K.T. Wang, X.-M. Cui, Study on the preparation of a free-sintered inorganic polymer-based proppant using the suspensions solidification method, J. Cleaner Prod., 148 (2017) 276–282.
[9] A. Madi Balo, H. Rahier, A. Mobili, A. Katsiki, N. Fagel, U. Melo Chinje, D. Njopwouo, Metakaolin-based inorganic polymer synthesis using cotton shell ash as sole alkaline activator, Constr. Build. Mater., 191 (2018) 1011–1022.
[10] F.L. Fu, Q. Wang, Removal of heavy metal ions from wastewaters: a review, J. Environ. Manage., 92 (2011) 407–418.
[11] P.-S. Keng, S.-L. Lee, S.-T. Ha, Y.-T. Hung, S.-T. Ong, Removal of hazardous heavy metals from aqueous environment by low-cost adsorption materials, Environ. Chem. Lett., 12 (2014) 15–25.
[12] N.H. Abdullah, K. Shameli, E.C. Abdullah, L.C. Abdullah, Solid matrices for fabrication of magnetic iron oxide nanocomposites: synthesis, properties, and application for the adsorption of heavy metal ions and dyes, Composites, Part B, 162 (2019) 538–568.
[13] B.M. Ibrahim, N.A. Fakhre, Crown ether modification of starch for adsorption of heavy metals from synthetic wastewater, Int. J. Biol. Macromol., 123 (2019) 70–80.
[14] I. Kara, D. Tunc, F. Sayin, S.T. Akar, Study on the performance of metakaolin based geopolymer for Mn(II) and Co(II) removal, Appl. Clay Sci., 161 (2018) 184–193.
[15] I. Kara, D. Yilmazer, S.T. Akar, Metakaolin based geopolymer as an effective adsorbent for adsorption of zinc(II) and nickel(II) ions from aqueous solutions, Appl. Clay Sci., 139 (2017) 54–63.
[16] V. Nejadshafiee, M.R. Islami, Adsorption capacity of heavy metal ions using sultone-modified magnetic activated carbon as a bio-adsorbent, Mater. Sci. Eng., C, 101 (2019) 42–52.
[17] Z.L. Du, T. Zheng, P. Wang, Experimental and modelling studies on fixed bed adsorption for Cu(II) removal from aqueous solution by carboxyl modified jute fiber, Powder Technol., 338 (2018) 952–959.
[18] A.V. Dmitriev, E.V. Vladimirova, M.V. Kandaurov, D.G. Kellerman, A.Y. Chufarov, A.P. Tyutyunnik, Hollow spheres of $BiFeO_3$: synthesis and properties, J. Alloys Compd., 743 (2018) 654–657.
[19] H. Ge, H.B. Xu, T.Y. Lu, J. Li, H.S. Chen, J.D. Wan, Microfluidic production of porous carbon spheres with tunable size and pores, J. Colloid Interface Sci., 461 (2016) 168–172.
[20] Q. Tang, Y.-Y. Ge, K.-T. Wang, Y. He, X.-M. Cui, Preparation and characterization of porous metakaolin-based inorganic polymer spheres as an adsorbent, Mater. Des., 88 (2015) 1244–1249.
[21] X. Zhao, W. Li, F.G. Kong, H.L. Chen, Z.Q. Wang, S.X. Liu, C.D. Jin, Carbon spheres derived from biomass residue via ultrasonic spray pyrolysis for supercapacitors, Mater. Chem. Phys., 219 (2018) 461–467.
[22] Y.Y. Ge, Y. Yuan, K.T. Wang, Y. He, X.M. Cui, Preparation of geopolymer-based inorganic membrane for removing Ni^{2+} from wastewater, J. Hazard. Mater., 299 (2015) 711–718.
[23] C.M. Li, Y. He, Q. Tang, K.-T. Wang, X.-M. Cui, Study of the preparation of CdS on the surface of geopolymer spheres and photocatalyst performance, Mater. Chem. Phys., 178 (2016) 204–210.
[24] Y.Y. Ge, X.M. Cui, Y. Kong, Z.L. Li, Y. He, Q.Q. Zhou, Porous geopolymeric spheres for removal of Cu(II) from aqueous solution: synthesis and evaluation, J. Hazard. Mater., 283 (2015) 244–251.
[25] T. Luukkonen, M. Sarkkinen, K. Kemppainen, J. Rämö, U. Lassi, Metakaolin geopolymer characterization and application for ammonium removal from model solutions and landfill leachate, Appl. Clay Sci., 119 (2016) 266–276.
[26] T.W. Cheng, M.L. Lee, M.S. Ko, T.H. Ueng, S.F. Yang, The heavy metal adsorption characteristics on metakaolin-based geopolymer, Appl. Clay Sci., 56 (2012) 90–96.
[27] Q. Tang, K. Wang, M. Yaseen, Z. Tong, X. Cui, Synthesis of highly efficient porous inorganic polymer microspheres for the adsorptive removal of Pb(II) from wastewater, J. Cleaner Prod., 193 (2018) 351–362.
[28] B.-H. Mo, H. Zhu, X.-M. Cui, Y. He, S.-Y. Gong, Effect of curing temperature on geopolymerization of metakaolin-based geopolymers, Appl. Clay Sci., 99 (2014) 144–148.
[29] M. Basu, A.K. Guha, L. Ray, Adsorption of lead on lentil husk in fixed bed column bioreactor, Bioresour. Technol., 283 (2019) 86–95.
[30] S. Chatterjee, S. Mondal, S. De, Design and scaling up of fixed bed adsorption columns for lead removal by treated laterite, J. Cleaner Prod., 177 (2018) 760–774.
[31] M.H. Zhang, H. Dong, Z.F. Geng, Computational study of particle packing process and fluid flow inside Polydisperse cylindrical particles fixed beds, Powder Technol., 354 (2019) 19–29.
[32] J.J. Qu, T. Song, J.S. Liang, X. Bai, Y. Li, Y.N. Wei, S.Q. Huang, L.Y. Dong, Y. Jin, Adsorption of lead(II) from aqueous solution by modified Auricularia matrix waste: a fixed-bed column study, Ecotoxicol. Environ. Saf., 169 (2019) 722–729.